Macromolecules **2006,** *39,* 821−828

Dilute Solutions of Strongly Charged Flexible Polyelectrolytes in Poor Solvents: Molecular Dynamics Simulations with Explicit Solvent

Rakwoo Chang

Department of Chemistry, Kwangwoon University, Seoul 139-701, Republic of Korea

Arun Yethiraj*

Theoretical Chemistry Institute and Department of Chemistry, University of Wisconsin,
Madison, Wisconsin 53706

Received May 27, 2005; Revised Manuscript Received November 27, 2005

ABSTRACT: The behavior of dilute salt-free solutions of charged flexible polymer molecules in poor solvents is studied using molecular dynamics simulations. The polymer molecule is modeled as a chain of charged spheres, the counterions are modeled as charged spheres, and the solvent molecules are incorporated explicitly and modeled as uncharged spheres. The pearl-necklace structures predicted by theory and observed in simulations with implicit solvent are not clearly seen in snapshots of chain conformations, although there is a clustering of monomers. An analysis of the single chain structure factor using a Kratky plot is misleading and not consistent with an analysis of cluster formation or a visual examination of snapshots. The conformational dynamics, as manifested in the decay of the intermediate scattering function, is relatively insensitive to solvent quality, except for the poorest solvent conditions. In this case the single chain structure factor displays oscillations, and the intermediate scattering function displays a dynamic slowing down at corresponding wavevectors. The simulations suggest that the presence of explicit solvent molecules can be an important aspect of polyelectrolyte behavior in poor solvents.

I. Introduction

The majority of polymers are composed of hydrophobic backbones and therefore do not dissolve in water. If they are synthesized with ionizable groups that dissociate in solution, however, the resulting electrostatic repulsion between the monomers prevents aggregation and precipitation. The balance between this electrostatic repulsion and the solvent-induced attractive interaction in polyelectrolyte solutions results in interesting static and dynamic properties that have been the focus of considerable research.[1−4] For example, while charged polymers are extended in good solvents and uncharged polymers are collapsed into spherical globules in poor solvents, charged polymers in poor solvents can display conformations intermediate to these extreme cases.

The conformational properties of isolated polyelectrolyte molecules in poor solvents are of current interest. Kantor and Kardar[5,6] argued that a collapsed spherical globule would be unstable with respect to capillary wave fluctuations, which make a charged liquid droplet split into smaller droplets.[7] They therefore suggested that the polyions would assume necklace-like conformations with collapsed globules joined by long thin strings. Dobrynin, Rubinstein, and Obukhov[8] developed a scaling theory based on this necklace model and predicted a cascade of abrupt transitions between necklace-like conformations with different numbers of globules. This model, which replaces the cylindrical model of polyion conformations suggested previously,[9−11] has captured the imagination of the polyelectrolyte community. A number of computer simulations of single polyions have been reported[8,12−19] where the pairwise additive site−site interaction consists of the sum of a Coulomb repulsion and a short-ranged attractive potential (to mimic the effect of the poor solvent). These simulations support the bead-necklace structure and sequence of transitions predicted by theory.

Experimental verification of the bead-necklace structure has, however, been elusive. While there have been many experiments on dilute solutions of synthetic polyelectrolytes,[20−23] using a number of different techniques, including viscometry, potentiometry, light scattering, X-ray diffraction, and neutron scattering, it has not been possible to obtain a definitive marker of the bead-necklace structure. Recently, Minko et al.[24,25] studied poly(2-vinylpyridine) adsorbed on a solid mica surface by atomic force microscopy (AFM) and reported that single polyelectrolyte molecules show a variety of different conformations ranging from a wormlike chain to a pearl-necklace-like conformation and finally a compact globule as the ionic strength of solution is increased, consistent with the theoretical predictions. Similar results were also obtained by Kirwan et al.,[26] who investigated the collapse of poly(vinylamine) molecules induced by variations in the solution pH. A caveat, however, is that the conformations of an adsorbed polymer are expected to be significantly different from those in bulk solution.[27] Therefore these experiments, although suggestive, are not conclusive regarding polyion conformations in solution.

In this work we revisit the problem of single polyelectrolyte chains in poor solvents using molecular dynamics simulations with the solvent molecules incorporated explicitly. Previous simulations for the collapse dynamics of neutral polymers[28] and semidilute polyelectrolytes in poor solvents[29] have demonstrated the importance of explicitly incorporating solvent molecules in strongly coupled systems. In particular, the stability of a locally collapsed globular conformation is artificially enhanced with implicit solvent because the solvent-induced attraction is present even between interior sites of the globule, where no solvent molecules are present. The solvent-induced effect is therefore patently many-body in nature, with exterior sites experiencing a different interaction than interior sites, an effect that is not present in implicit solvent models.

10.1021/ma051095y CCC: $33.50

Our main result is that we do not observe bead-necklace structures in snapshots taken from the simulations. An analysis of the conformations using cluster algorithms, however, gives results that are consistent with the theoretical predictions. In our simulations, the globules are held together quite loosely and are therefore much more mobile and dynamic objects than might be inferred from previous simulations. Many static properties of our model, such as the average chain size, are similar to those obtained from implicit solvent models, but some dynamic properties are quite different.

The rest of this paper is organized as follows. In section II we describe the molecular model and simulation details, in section III we present and discuss static and dynamic properties, and in section IV we summarize our results and present some conclusions.

II. Molecular Dynamics Simulations

A. Molecular Model. The molecular model is similar to that used in previous work.[29] The polyion is composed of uniformly charged monomers connected by finitely extensible nonlinear elastic (FENE) springs. The counterions are modeled as spheres of the same size and magnitude of charge (but opposite sign) as the monomers of the chain. Solvent molecules are included explicitly as a third component, which are modeled as uncharged spheres. The interaction potential, $V_{ij}(r)$, between sites i and j is given by

$$V_{ij}(r) = k_B T \frac{Z_i Z_j l_B}{r} + \lambda_{ij} V_{LJ}(r) + (1 - \lambda_{ij}) V_{WCA}(r) \quad (1)$$

where k_B is Boltzmann's constant, T is the temperature, Z_i is the charge valence of sites of species i, i.e., $Z_i = +1, -1$, and 0 for monomer, counterion, and solvent sites, respectively, and l_B is the Bjerrum length, defined by

$$l_B = \frac{e^2}{\epsilon k_B T} \quad (2)$$

where e is the unit charge and ϵ is the dielectric constant of solvent. In the above, $V_{LJ}(r)$ is the Lennard-Jones (LJ) potential, truncated at 2.5σ and shifted, where σ is the LJ collision diameter, and $V_{WCA}(r)$ is the repulsive LJ potential truncated at $2^{1/6}\sigma$ and shifted. The λ_{ij} are solvent quality parameters given by $\lambda_{mm} = \lambda_{ss} = \lambda$, and $\lambda_{ij} = 0$ for all other pairs of i and j, where "m" stands for monomer and "s" for solvent. The Ewald summation method is used for handling the long-range nature of the Coulomb potential.

The bonding potential between neighboring beads along the polymer backbone, $V_F(r)$, is given by

$$V_F(r) = -\frac{1}{2} k_F {R_0}^2 \ln\left(1 - \frac{r^2}{{R_0}^2}\right) \quad (3)$$

where k_F is the spring constant and R_0 is the maximum extension of the bond. In this simulation, we use $k_F = 30.0 k_B T/\sigma^2$ and $R_0 = 1.5\sigma$; these parameter values prevent bond crossing.

The solvent quality is modified by changing the parameter λ. The nonelectrostatic contribution to the monomer−solvent, monomer−counterion, counterion−counterion, and counterion−solvent potentials is purely repulsive and accounts for excluded volume. However, the nonelectrostatic contribution to the monomer−monomer and solvent−solvent potentials becomes attractive as λ is increased. When λ is equal to 0, all nonelectrostatic interactions are identical, and therefore the solvent quality is good. On the other hand, when λ is equal to 1, the attractions between monomers and between solvent molecules make the solvent quality poor;[28] the solvent quality is changed by tuning λ between 0 and 1. The advantage of using this potential instead of the Lennard-Jones potential is that the repulsive part does not change appreciably with λ. As shown in our previous study,[28] this choice of interaction allows one to use larger time steps in molecular dynamics simulations.

B. Simulation Method. The simulation cell is a cube of side length L with periodic boundary conditions in all directions. We study *single* polyelectrolyte chains with degrees of polymerization, $N_m = 16$, 32, and 64 with the same number of counterions for charge neutrality. In some cases (especially in poor solvent conditions) we also investigate $N_m = 128$ and 256. The box length L is chosen such that the monomer density $\rho_m\sigma^3$ is ∼0.004. For example, $L = 16\sigma$, 20σ, and 25σ were used for $N_m = 16$, 32, and 64, respectively. In most cases, $\rho_m\sigma^3 = 0.004$, but to study possible finite size effects, we also perform simulations of $N_m = 16$ for $\rho_m\sigma^3 = 0.001$. Solvent atoms are added to the simulation box to make the total density $\rho_{tot}\sigma^3 = 0.864$. Lengths are measured in units of σ, time in units of $\tau_{MD} = (m\sigma^2/\epsilon_{LJ})^{1/2}$, and temperature in units of ϵ_{LJ}/k_B. For simplicity, we henceforth set the three parameters, m, σ, and ϵ_{LJ}, equal to unity and defined a reduced temperature, $T^* \equiv k_B T/\epsilon_{LJ}$. In the present study $T^* = 1.0$.

The molecular dynamics simulation method is a standard application of existing techniques, and the reader is referred to a previous paper for details.[29] Initial configurations are generated with the atoms on the lattice points of a face-centered-cubic structure with N_m adjacent vertices chosen for the polyion. Initial velocities are generated via a Gaussian random number generator and scaled to give the desired temperature. The system is evolved using the explicit reversible integrator[30−32] with the Nosé-Hoover thermostat,[33,34] with an integration time step of $0.005\tau_{MD}$ and a Nosé-Hoover coupling constant of 5. Initial conformations are considered to be equilibrated when the total energy, system temperature, and the chain size do not drift. After equilibration, trajectories of polyions, counterions, and solvents are sampled every 1000 time steps ($5\tau_{MD}$), and statistical averages are obtained over 1000−3000 configurations. The average bond length between monomers in a polyelectrolyte chain was constant (=0.965) for all λ.

III. Results and Discussion

A. Chain Dimensions. The scaling of chain size with the degree of polymerization has been studied extensively.[27] In good solvents, electrostatic effects dominate, and the mean-square radius of gyration, $\langle {R_g}^2 \rangle$, scales as ${N_m}^{2\nu}$ with $\nu = 1$: i.e., the chain is extended (provided counterion-mediated attractions are not significant). In very poor solvents, solvent-induced effects dominate, and the chain is collapsed, and $\nu \approx 1/3$. In solvents of intermediate quality the balance between electrostatic and solvent-induced effects is more subtle. According to the theory of Dobrynin et al.,[8,35,36] the chains form a necklace of blobs. The molecules are locally collapsed, but these blobs are arranged so that the scaling with N_m is the same as in good solvents. The results of the chain size obtained from our model are consistent with what has been observed in previous simulations with explicit counterions but implicit solvent.

We first estimate the θ solvent condition for our model from simulations of neutral chains. Figure 1a depicts $\langle {R_g}^2 \rangle$ (normalized by N_m) as a function of N_m for neutral chains for various values of λ. In a θ solvent, $\langle {R_g}^2 \rangle \sim N_m$ and the curve in Figure 1a will be flat. We find that this happens for $\lambda = 0.1$, where $\langle {R_g}^2 \rangle/N_m$

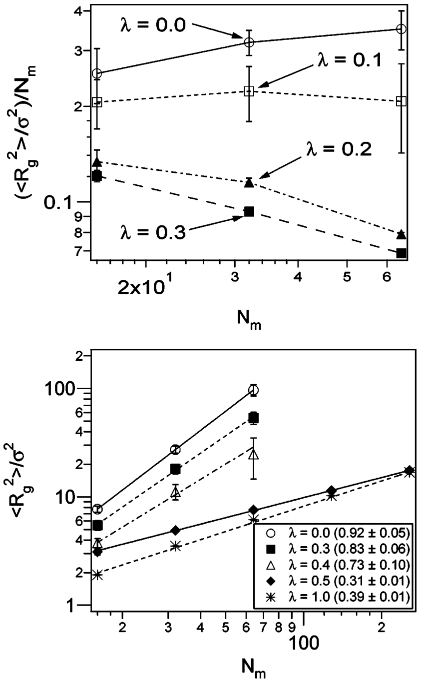

Figure 1. (a) $\langle R_g^2\rangle/N_m$ of a neutral chain as a function of N_m for various values of λ. The θ solvent condition, where $R^2 \sim N_m$, occurs for $\lambda \approx 0.1$. (b) A log−log plot of $\langle R_g^2\rangle$ as a function of N_m for a charged chain ($l_B = 1$) for various values of λ. The slope of each line and statistical uncertainties are shown in parentheses in the legend, for each value of λ.

is almost independent of N_m in the range of $N_m = 16-64$. We identify $\lambda = 0.1$ as the θ point for this model. The slight negative curvature seen for $\lambda = 0.0$ and 0.1 may be attributed to the finite size of the simulation box and the finite concentration of polymer molecules. Since the monomer concentration is fixed at $\rho_m\sigma^3 = 0.004$, the simulation box linear dimension only increases as $N_m^{1/3}$ with increasing N_m. In good and θ solvents, the longer chains "feel" the edges of the box more than the shorter chains. In addition, the overlap threshold concentration, ρ_m^*, scales as $N_m^{-4/5}$, and the longer chains are therefore closer to ρ_m^* than the shorter chains.

The overlap threshold concentration can be estimated from[37]

$$\rho_m^* = \frac{0.64N_m}{\frac{\pi}{6}R^3} \tag{4}$$

where R is the root mean-square end-to-end distance. For neutral chains and for $\rho_m\sigma^3 = 0.004$ and $\lambda = 0$, $R = 4.69$, 7.96, and 11.85 for $N_m = 16$, 32, and 64, respectively, with corresponding values of $\rho_m^* = 0.189$, 0.0775, and 0.0470. For charged chains and for $\rho_m\sigma^3 = 0.004$ and $\lambda = 0$, $R = 7.58$, 15.0, and 28.7 for $N_m = 16$, 32, and 64, respectively, with corresponding values of $\rho_m^* = 0.180$, 0.0232, and 0.00330. For charged chains $\rho_m^* \sim N_m^{-2}$ and is therefore a much stronger function of the degree of polymerization. With this estimate of ρ_m^*, the concentration of neutral chains is below ρ_m^* but charged chains with $N_m \geq 64$ may be interpreted to be in the semidilute regime for $\lambda = 0$.

We do not believe the proximity to the overlap threshold concentration to be significant. It is important to emphasize that this is just an estimate of the overlap threshold concentration, i.e., the concentration in a real solution where chains are likely to interact with other molecules on average. In the simulations, however, we have only one chain, and its distance from periodic images is always constant. In any event, in poor solvents the size of the chain is much smaller, and therefore ρ_m^* will be much higher than in good solvents. In fact, the applicability of these scaling ideas for poor and marginal solvents has been questioned,[38] and they should not be taken literally. It is more important to establish that finite size effects do not play a significant role. We have studied different system sizes (as described in the previous section) to estimate finite size effects, for $N_m = 16$.

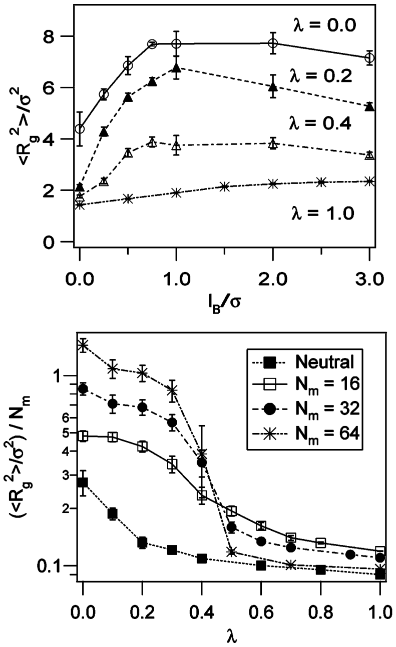

Figure 2. $\langle R_g^2\rangle$ as a function of (a) l_B for various values of λ and $N_m = 16$ and (b) λ for various values of N_m and $l_B = 1$. In (b) the result for a neutral chain with $N_m = 16$ is also shown for comparison.

The value of the scaling exponent ν decreases as the solvent quality is decreased. Figure 1b depicts the variation of $\langle R_g^2\rangle$ with N_m (on a logarithmic plot) for various values of λ and for $l_B/\sigma = 1$. The legend shows the slope of the lines. There are several features worth noting. $\langle R_g^2\rangle$ does not grow linearly with N_m for $\lambda = 0$, although it is extended compared to the neutral chain. This contraction relative to the expected behavior could be due to the finite size effects mentioned above. Note, however, that the effective solvent-mediated potential between polymer beads is attractive even for $\lambda = 0$; i.e., the effective potential between monomer beads with explicit solvents is more attractive than that without solvent atoms.[39] As λ is increased, the scaling exponent decreases, with $\nu \approx 0.83$, 0.73, and 0.31 for $\lambda = 0.3$, 0.4, and 0.5, respectively. Interestingly, the scaling exponent for $\lambda = 0.5$, $\nu = 0.31$, is even smaller than that of collapsed chains and is related to the chain-length dependence of the collapse transition regime. The collapse transition is known to have a finite transition range, which scales as $1/\sqrt{N_m}$.[40] For $\lambda = 0.5$, the chain is not completely collapsed for $N_m = 16$ but is completely collapsed for $N_m = 64$.

The size of an isolated polyion displays a nonmonotonic dependence on the strength of the electrostatic interaction, l_B, in good solvents but increases monotonically with l_B in very poor solvents. Figure 2a depicts the mean-square radius of gyration, $\langle R_g^2\rangle$, as a function of l_B for $N_m = 16$ and for various solvent conditions. In most cases, a nonmonotonic dependence of $\langle R_g^2\rangle$ on l_B is observed, with the peak occurring for $l_B \sim \sigma$. For small values of l_B the chain properties are dominated by the repulsion between the monomers. In this regime, increasing l_B results in an increase in the chain size. For large values of l_B, the correlations between monomers and counterions become

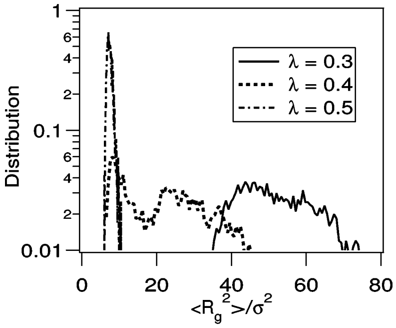

Figure 3. Distribution of chain sizes for $N_m = 64$ and various values of λ (as marked).

important. In this regime, increasing l_B results in a decrease in chain size because the correlations between counterions cause them to induce attractions between monomers beads, either by forming dipoles with monomers or by acting as ionic bridges. Such behavior has been reported previously.[37,41–43] In very poor solvents, however, increasing l_B results in a monotonic increase in $\langle R_g^2 \rangle$ for all values of l_B. This is because more counterions are in the immediate vicinity of the polyion as l_B is increased, and this has the effect of swelling the polymer.

The polymer size decreases monotonically as the solvent quality is decreased, as expected. Figure 2b depicts $\langle R_g^2 \rangle$ divided by the degree of polymerization, N_m, as a function of the solvent quality, λ, for $N_m = 16$, 32, and 64 and for $l_B/\sigma = 1$. Also shown, for comparison, is the behavior of a neutral chain for $N_m = 16$ with the same nonelectrostatic interactions as the charged chain. For all values of λ (for $N_m = 16$) a charged chain has a larger size than a neutral chain. When the solvent-induced interaction is either weak or absent (e.g., $\lambda = 0$ and 0.2), the polyion size is larger than a neutral chain by the factor of 2−3, and this size difference decreases as λ is increased. However, the polyion never achieves the same size as the neutral chain, even for very poor solvents ($\lambda = 1$). This is because in poor solvents the counterions are present in the interior of the collapsed globule, and this tends to swell the chain relative to the neutral chain. The transition from an extended to a globular state moves to higher value of λ in a charged chain when compared to a neutral chain of the same length. In addition, for charged chains, the value of λ at which the collapse transition occurs does not depend on the degree of polymerization, N_m, although the transition is sharper for longer chains.

There has been some discussion regarding the order of the polyelectrolyte collapse transition[44] with suggestions that the transition is continuous for neutral chains and discontinuous for charged chains. A bimodal size distribution, which is the evidence of the discontinuous or the first-order transition of a single polyelectrolyte chain, has been observed by experiments[45,46] and simulations without explicit counterions.[12] Of course, a truly discontinuous transition occurs only in the limit of $N_m \to \infty$, and it is difficult to examine the order of the transition in simulations of chains with finite length. An examination of the distribution of chain sizes does, however, shed light on the issue. Figure 3 depicts the probability distribution of $\langle R_g^2 \rangle$ for $N_m = 64$ and various values of λ. For $\lambda = 0.3$ and 0.5, the chain is extended and collapsed, respectively, and the distribution shows one peak near $R_g^2 \approx 45$ and 10, respectively. For $\lambda = 0.4$, i.e., solvent condition near the collapse transition, the distribution is bimodal with two peaks clearly distinguishable. This is similar to what is observed in simulations without explicit solvent but with explicit counterions.[16–19] It should be mentioned that the bimodal distribution is not observed for chain lengths of $N_m = 16$ and 32 because the collapsed and extended states are too similar in size.

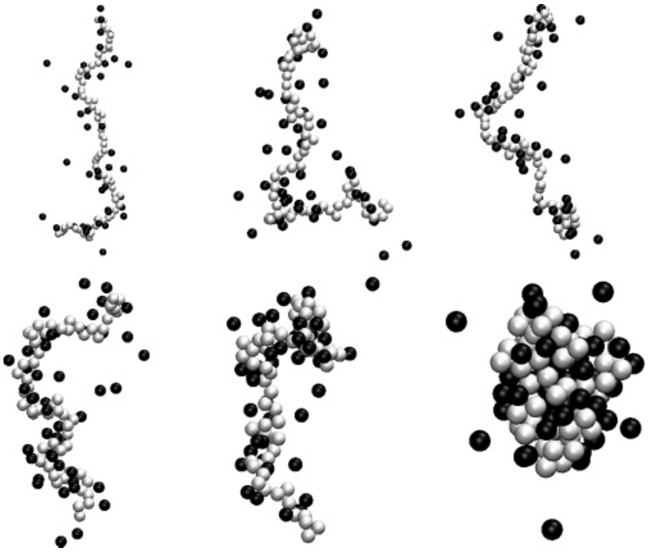

Figure 4. Representative snapshots of a polyion (white) with $N_m = 64$ and counterions (black) within 5σ from the chain for $\lambda = 0.0$, 0.1, 0.2, 0.3, 0.4, and 0.5 (from upper left) and $l_B = \sigma$. Solvent molecules are omitted for clarity.

The qualitative behavior of the chain conformations is not sensitive to the polymer concentration in the dilute regime. Although there is only one polymer molecule in the simulation cell, the monomer concentration is finite because of the finite size of the simulation cell. In the results presented thus far, the monomer concentration was set to $\rho_m\sigma^3 = 0.004$. Of course, the monomer concentration is an important parameter because as ρ_m decreases, the entropic effect causes more counterions to leave the region near the polymer; in the *infinite* dilution limit, the counterions would leave the polymer entirely. This leads to the weaker screening of the intramolecular electrostatic repulsion, and the collapse transition should occur for a large value of λ (or poorer solvent condition). We observe these effects in simulations for $\rho_m\sigma^3 = 0.001$, and we do not show these results because the qualitative behavior is the same for $\rho_m\sigma^3 = 0.001$ and 0.004. Note that, unlike implicit solvent models, the computational cost of our explicit solvent model approximately scales as $1/\rho_m$, which places limits on the monomer concentrations that we can investigate.

B. Bead-Necklace Formation. Scaling theories[8,35,36] predict that a single polyelectrolyte chain forms a necklace of blobs in poor solvents, a prediction that has been supported by many computer simulations[8,12–15] of polyelectrolytes without an explicit treatment of the solvent. As the solvent quality is decreased, these blobs coalesce to eventually form a spherical globule in very poor solvents.

We do not see distinct signatures of these pearl-necklace structures in our simulations. Figure 4 depicts representative snapshots of a single polyelectrolyte chain for various values of λ, $l_B = \sigma$, and $N_m = 64$. As the solvent quality is decreased, the monomers on the chains begin to cluster. In some cases, we do see a dumbbell structure (see snapshot for $\lambda = 0.4$) which is similar to the pearl-necklace structure. However, under these conditions the polymer chain undergoes significant conformational fluctuations, and shapes such as amorphous globules, extended strings, and sausage-like shapes are also observed. Therefore, we cannot claim that the dumbbell structure is the most dominant structure, let alone the only conformation.

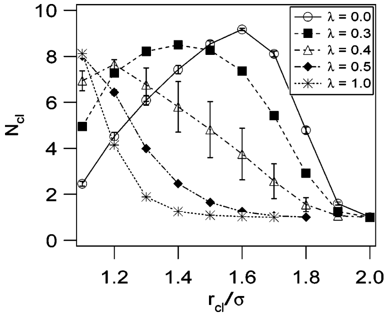

Figure 5. Number of clusters, N_{cl}, as a function of the cutoff distance, r_{cl}, for $N_m = 64$ and various values of λ.

To investigate the pearl-necklace structure formation more systematically, we monitor the number and the size of clusters in a single polymer chain using the nearest-neighbor distance criterion of Stoddard.[47,48] Two nonbonded beads are considered to be in the same cluster if they are closer than r_{cl}, where r_{cl} is the critical bead separation. For atomic clusters where there is no bond between atoms, the appropriate r_{cl} is in the range of $1.3\sigma-1.8\sigma$.[48] However, for clusters within a single polymer chain, r_{cl} should be chosen such that two beads connected by two bonds are not identified as a cluster unless they are close enough. In fact, the number of clusters, N_{cl}, is strongly dependent on r_{cl}, and a careful choice of this parameter is important. Figure 5 depicts the number of clusters as a function of the cutoff distance r_{cl} for $N_m = 64$, $l_B/\sigma = 1$, and various values of λ. The variation of N_{cl} with r_{cl} is different depending on the chain conformation: it decreases monotonically for collapsed chains ($\lambda = 0.5$ and 1.0), but has a maximum in other cases ($\lambda = 0.0$, 0.3, and 0.4). The initial increase in N_{cl} for extended chains reflects that clusters are bound loosely by weak solvent-mediated interactions. The decrease of N_{cl} for both extended and collapsed chains can be explained by the fact that neighboring clusters merge as r_{cl} is increased, thus resulting in the smaller number of clusters.

An analysis of the clustering of monomers provides a picture that is qualitatively consistent with the idea of bead-necklace formation. To analyze conformations in terms of clusters, we set $r_{cl} = 1.2\sqrt[6]{2}\sigma \equiv 1.347\sigma$, which guarantees that beads separated by two bonds are in the same cluster only if the angle between these two bonds is approximately less than 90°.

Parts a and b of Figure 6 depict respectively the number of clusters per monomer bead, N_{cl}/N_m, and the number of monomers in each cluster, S_{cl}, as a function of λ for $l_B = \sigma$. The results for a neutral chain with $N_m = 16$ are also shown for comparison. (Note that the ordinate in Figure 6b is drawn on a logarithmic scale.) There are several notable features. First of all, N_{cl} increases as λ is increased from 0 to 0.3 and starts decreasing rapidly for larger values of λ. This is in contrast to neutral chains where the number of clusters decreases monotonically for all ranges of λ. This maximum occurs just prior to the collapse transition and can be explained as follows. When λ is increased, the polyelectrolyte chain starts forming local globules usurping nearby loose monomers until no loose beads are left, and this leads to an increase in both N_{cl} and S_{cl}. When λ is further increased, those local globules coalesce to make fewer globules, which results in the decrease in N_{cl} and an increase in S_{cl}. Second, N_{cl}/N_m for various chain lengths coincides at low λ: i.e., N_{cl} increases linearly with N_m for weak hydrophobic interactions ($\lambda < 0.4$). On the other hand, S_{cl} does not depend on N_m in this range of λ, as shown in Figure 6b. These findings strongly suggest that clusters in a polyelectrolyte chain are formed locally in short length scales, unaffected by the whole chain size in weakly poor solvents. In the strong hydrophobic interaction regime ($\lambda > 0.4$), both N_{cl}/N_m and S_{cl} are, however, dependent on the chain length, indicating a global conformational change. In fact, the total number of monomer beads participating in clusters, divided by the chain length, is independent of the chain length in this regime (not shown).

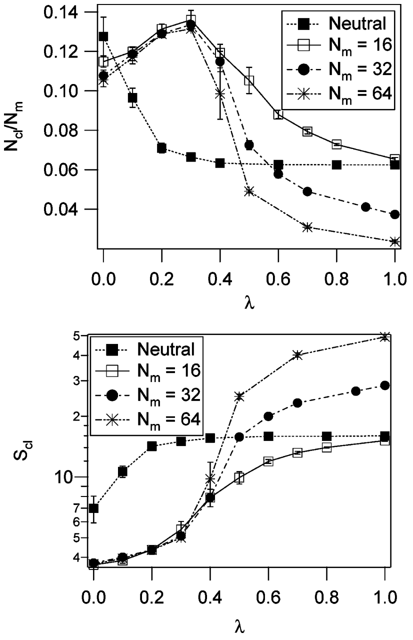

Figure 6. (a) Number of clusters, N_{cl}, and (b) the average number of monomer beads per cluster, S_{cl}, as a function of solvent quality, λ, for various N_m. Two beads belong to the same cluster if their separation is less than $1.2\sqrt[6]{2}\sigma \equiv 1.347\sigma$.

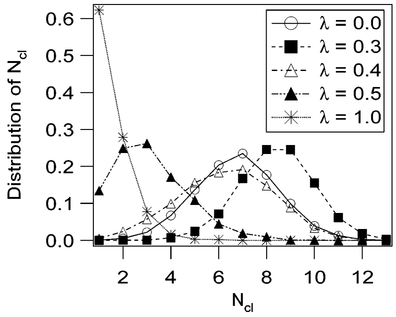

Figure 7. Distribution of N_{cl} for $N_m = 64$ and various λ.

Another important distinction between the conformations seen in these simulations and those in previous work with implicit solvent is that the monomers in the bead structure are held together in a fairly loose fashion in this work compared to what has been observed previously. The breaking up and re-forming of the beads occur fairly rapidly because the only driving force is the surface tension of the solvent (there is no artificially strong attractive interaction between polymer beads). This could be a reason why these structures are difficult to observe experimentally.

The loose nature of the cluster formation results in a distribution of N_{cl} that is considerably broad, except when the chain is collapsed. Figure 7 depicts the distribution of N_{cl} for $N_m = 64$ and $l_B = \sigma$. The peak of the distribution moves to higher values as λ is increased to 0.3 and then moves to lower values as λ is increased further. Note that the width of the distribution for $\lambda = 0.0$ is almost the same as that for $\lambda = 0.4$, which is near the collapse transition. Incidentally, a bimodal distribution of N_{cl} is not observed for $\lambda = 0.4$, in contrast to

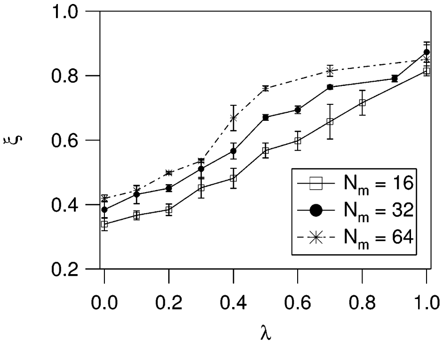

Figure 8. Fraction of "condensed" counterions, ξ, as a function of solvent quality. A counterion is considered to be condensed if it is within 2.5σ of the nearest polymer site.

the distribution of the polymer size. We also do not observe any distinctive transition between different numbers of pearl-necklace structures, although we cannot rule out the possibility of those transitions for much longer chains.

C. Counterion Distribution. In the original version of the counterion condensation theory,[49] when an infinitely thin charge rod is placed in solution, the free energy diverges for sufficiently high polyelectrolyte charge densities. This divergence would be avoided if counterions condense or collapse onto the rod thus reducing the charge density. Although the condensation of this nature cannot occur in systems with finite excluded volume, the correlations between counterions and polyions are expected to become stronger as the solvent quality is decreased. We define a parameter ξ to estimate the degree of counterion correlation

$$\xi = \frac{N_{\mathrm{con}}}{N_{\mathrm{c}}} \tag{5}$$

where N_{con} is the number of counterions within a certain cutoff distance, $r_{\mathrm{c}}^{\mathrm{cc}}$, from any monomer on the chain, and N_{c} is the total number of counterions. Figure 8 depicts ξ as a function of λ for $N_{\mathrm{m}} = 16$, 32, and 64 with $r_{\mathrm{c}}^{\mathrm{cc}} = 2.5\sigma$. (The results are qualitatively similar for other reasonable values of the cutoff in the range $\sigma < r_{\mathrm{c}}^{\mathrm{cc}} < 4\sigma$.) As λ is increased, ξ also increases, with the same trend for all degrees of polymerization. This is because the decrease of the solvent quality causes the polyelectrolyte chain to contract, thus increasing the electrostatic repulsion between monomer beads, which promotes the "condensation" of counterions. What is interesting is that when $\lambda > 0.6$, ξ continues to increase although the chain size remains constant; for $\lambda = 1.0$, about 80% of counterions are localized near the collapsed chain. Considering that the monomer concentration is 0.004, which is in the dilute regime, this high percentage of condensed counterions is mainly due to the strong electrostatic correlation between monomers and counterions.

D. Static and Dynamic Structure Factors. The intramolecular static structure factor (or the form factor), $\hat{\omega}(k)$, is defined by

$$\hat{\omega}(k) = \frac{1}{N_{\mathrm{m}}} \sum_{i,j}^{N_{\mathrm{m}}} \left\langle \frac{\sin(kr_{ij})}{kr_{ij}} \right\rangle \tag{6}$$

where N_{m} is the degree of polymerization and r_{ij} is the distance between the ith and jth monomers in a single chain. The intramolecular intermediate scattering function, $\hat{F}(k,t)$, is the spatial Fourier transform of the corresponding van Hove function and is defined by

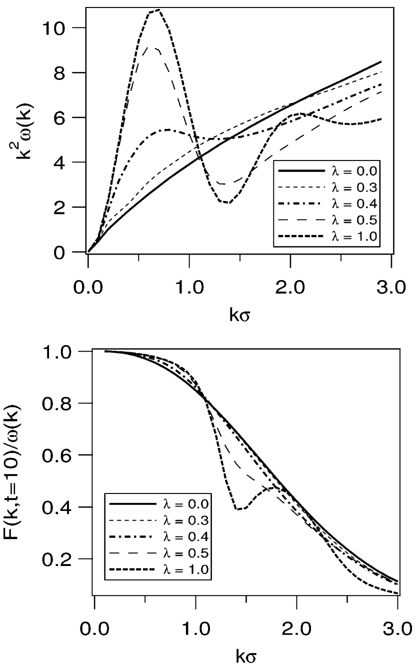

Figure 9. (a) Static intramolecular structure factor, $\hat{\omega}(k)$, of a 64-bead chain (multiplied by k^2) for various λ. (b) Intramolecular intermediate scattering function, $\hat{F}(k,t)$, normalized by its static component, $\hat{\omega}(k)$, for a time $t = 10$, for various values λ and $l_{\mathrm{B}} = \sigma$.

$$\hat{F}(k,t) = \frac{1}{N_{\mathrm{m}}} \sum_{i,j}^{N_{\mathrm{m}}} \left\langle \frac{\sin(kr_{ij}(t))}{kr_{ij}(t)} \right\rangle \tag{7}$$

where $r_{ij}(t) \equiv |\mathbf{r}_i(t) - \mathbf{r}_j(0)|$ is the distance between the ith monomer at time t and the jth monomer at time 0. Therefore, $\hat{\omega}(k)$ is equal to $\hat{F}(k,t)$ at time $t = 0$. The functions $\hat{\omega}(k)$ and $\hat{F}(k,t)$ are calculated using methods described elsewhere.[43]

Figure 9a,b depicts the single chain static and dynamic structural properties for $N_{\mathrm{m}} = 64$ and $l_{\mathrm{B}}/\sigma = 1$ and for various values of λ. Figure 9a depicts the single chain structure factor plotted in the standard Kratky form. In the scaling regime, $\hat{\omega}(k)$ scales as k^{-2} and k^{-1} for ideal chains and rods, respectively, and a (Kratky) plot of $k^2\hat{\omega}(k)$ vs k therefore displays a plateau for ideal chains and is an increasing function of k for rods. For $\lambda = 0$ and 0.3, $k^2\hat{\omega}(k)$ is an increasing function of k in the scaling regime, for $\lambda = 0.4$, there is a plateau reminiscent of the behavior of an ideal chain, and for $\lambda = 0.5$ and 1.0, a prominent peak in $k^2\hat{\omega}(k)$ is manifest for $k\sigma \approx 0.7$. For $\lambda = 1.0$, a second peak is present for $k\sigma \approx 2$. This behavior is consistent with the chains being extended for low values of λ, being close to ideal for intermediate values of λ, and being collapsed globules for high values of λ. The analysis of the cluster formation and visual examination of snapshots of configurations provide a rather different picture of chain conformations, however, suggesting that the single chain structure factor does not provide sufficiently detailed information on chain conformational behavior. Similar conclusions were reached in the analysis of simulations of two-dimensional polymer chains.[50]

The structural correlation (or ordering) at $k\sigma \approx 2$ for $\lambda = 1.0$ has a significant effect on the conformational relaxation of the chain at that length scale. Figure 9b depicts the intramolecular intermediate scattering function, $\hat{F}(k,t)$, normalized by $\hat{\omega}(k)$, as a function of wavevector at time $t = 10$ for various values of λ. The figure clearly shows that the relaxation of the density–

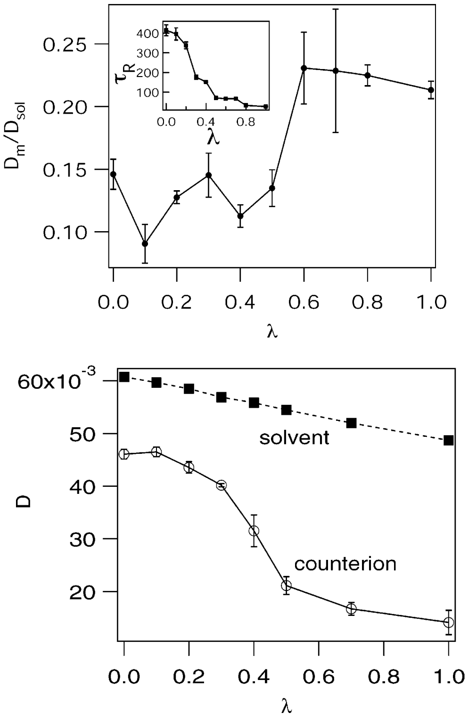

Figure 10. Self-diffusion coefficients, D, of (a) polyions, (b) counterions, and solvent atoms as a function of λ, for $N_m = 64$ and $l_B = \sigma$. In (a), the polyion diffusion coefficient, D_m, is scaled by the solvent diffusion coefficient, D_{sol}. The inset in (a) is the rotational relaxation time, τ_R, of the end-to-end distance, R_e, of polyions. τ_R was obtained by fitting the time correlation function of R_e using $A \exp(-t/\tau_R) + B$.

density correlation for $k\sigma \approx 2$ is slowed down for $\lambda = 1.0$. Notice that $\hat{F}(k,t)/\hat{\omega}(k)$ for $\lambda = 0.5$ shows no sign of slowing down although the size of the chain at $\lambda = 0.5$ is almost the same as that at $\lambda = 1.0$. This suggests that the collapsed chain is much more mobile and flexible for $\lambda = 0.5$ than for $\lambda = 1.0$.

E. Diffusion Coefficients. The long-time self-diffusion coefficients of counterions and solvent atoms are calculated using the Einstein relation

$$D = \lim_{t\to\infty} \langle (r_i(t) - r_i(0))^2 \rangle / 6t \qquad (8)$$

where $r_i(t)$ is the position of the ith particle at time t. The diffusion coefficient of the center of mass of polyions, D_m, relative to the solvent diffusion coefficient, D_{sol}, is depicted in Figure 10a for $N_m = 64$ and $l_B = \sigma$. Since there is only one polyion in the simulation box, the statistical uncertainties are large. Nevertheless, the general trend is clear: collapsed chains in the range of $\lambda = 0.6-1.0$ have a higher diffusion coefficient than extended chains. This is expected because the diffusion is inversely proportional to the hydrodynamic radius of polyion chains. The effect of the chain size on the dynamics is more pronounced in the rotational motion of polyions. The rotational relaxation time, τ_R, of the end-to-end distance, R_e, of polyions is shown in the inset of Figure 10a. (τ_R is obtained by fitting the time correlation function of R_e using $A \exp(-t/\tau_R) + B$.) Since τ_R scales as R^2, collapsed chains relaxes an order of magnitude faster than extended chains.

The self-diffusion coefficients of counterions and solvent atoms are shown in Figure 10b for $N_m = 64$ and $l_B = \sigma$. The counterion self-diffusion is slower than the solvent atoms for all values of λ, and the solvent dynamics is only weakly dependent on λ. This is expected because counterions are strongly attracted to the polyelectrolyte chain by the electrostatic interaction. Although there is no permanent trapping, it slows down the translational motion of counterions. Therefore, the behavior of the self-diffusion of counterions is closely related to the correlations between counterions and polyions. This is clearly seen from Figures 8 and 10, where the functional form of these two properties as a function of solvent quality (or λ) shows a similar shape.

IV. Summary and Conclusions

Molecular dynamics simulations are presented for the properties of dilute solutions of salt-free flexible polyelectrolytes in poor solvents. Results for the average chain size are similar to what is seen in simulations with explicit counterions but with implicit solvent. For example, the size of polyelectrolyte chains shows a nonmonotonic dependence on the Bjerrum length in good and slightly poor solvents but monotonically increases with the Bjerrum length in very poor solvents. For very poor solvents the chain collapses accompanied by the migration of counterions to the vicinity of the collapsed globule. Consequently, the size of the collapsed polyelectrolyte chain is always larger than that of a neutral chain.

We do not see clear signatures of the pearl-necklace structure in snapshots from the simulations. However, an analysis of the cluster formation in the simulations suggests clustering consistent with the local cluster picture except that the blobs are very loosely held. The number of clusters in a single polyelectrolyte chain is a nonmonotonic function of the solvent quality. We interpret this to mean that as the solvent quality is decreased, polyelectrolyte chains form local cluster structures, and when the solvent quality is decreased further, the chain collapses into a spherical globule. The local cluster structures are loosely formed by the surface tension between monomers and solvent atoms. Consequently, the local cluster structure is not as stable as inferred from simulations without explicit solvent. As a caveat we note that, because we have finite simulation cells, the simulated polymer concentration is higher than in previous simulations with implicit solvent.

The single chain structure factor does not display signatures of the bead-necklace structure. A standard analysis of the single chain structure can be misleading and is not consistent with the more detailed information available in the simulations. In poor solvents, the single chain structure factor shows a peak near $k\sigma \approx 2$, which corresponds to a short length scale ordering of the monomers. The relaxation of the chains on these length scales is slowed down by this correlation effect.

The large statistical uncertainties notwithstanding, the simulations show that the polyion diffusion coefficient is clearly affected by the solvent quality. The counterion diffusion coefficient is also affected by the quality of solvent because the polyelectrolyte collapse induces more counterions to be condensed in the collapsed globule. The counterions are not dynamically localized, and the counterion self-diffusion coefficient varies by a factor of 5 over the range of solvent qualities investigated. The behavior of the counterion diffusion coefficient tracks that of the number of counterions in the vicinity of the polyion.

The effect of incorporating the solvent explicitly on the properties of polyelectrolytes in poor solvent can be significant. The nature of the pearl-necklace structure is quite different when the solvent is incorporated explicitly compared to previous studies. The main difference is that in simulation without explicit solvent the monomers in each cluster are strongly bound by strong pairwise attractions, hence making the structure very stable. With explicit solvent atoms the cluster is held together quite loosely and therefore breaks apart quite easily. This could explain why the pearl-necklace structure is difficult to observe experimentally, especially since no signature is seen in the static structure factor. As a caveat, we note that the solvent model used in this work by no means represents water in a realistic fashion. In particular, the solvent molecules do not alter the electrostatic interactions between ions, which depend only on the interion separation. Polarizability and local dielectric effects are not considered and could be an important aspect of real systems. This work suggests that incorporating solvent molecules explicitly could be important, and an investigation of more realistic explicit solvent models is therefore an important future direction.

Acknowledgment. We gratefully acknowledge support from the National Science Foundation (through Grant CHE 0315219 to A.Y. and Grant CHE 0091916 to the Department of Chemistry).

References and Notes

(1) Oosawa, F. *Polyelectrolytes*; Dekker: New York, 1971.
(2) Mandel, M. *Polyelectrolytes*; Reidel: Dordrecht, 1988.
(3) Hara, M. *Polyelectrolytes: Science and Technology*; Dekker: New York, 1993.
(4) Förster, S.; Schmidt, M. *Adv. Polym. Sci.* **1995**, *120*, 51−133.
(5) Kantor, Y.; Kardar, M. *Europhys. Lett.* **1994**, *27*, 643−648.
(6) Kantor, Y.; Kardar, M. *Phys. Rev. E* **1995**, *51*, 1299−1312.
(7) Rayleigh, L. *Philos. Mag.* **1882**, *14*, 184.
(8) Dobrynin, A. V.; Rubinstein, M. *Macromolecules* **1996**, *29*, 2974−2979.
(9) Khokhlov, A. R. *J. Phys. A: Math. Gen.* **1980**, *13*, 979−987.
(10) Raphael, E.; Joanny, J. F. *Europhys. Lett.* **1990**, *13*, 623.
(11) Higgs, P. G.; Orland, H. *J. Chem. Phys.* **1991**, *95*, 4506−4518.
(12) Lyulin, A. V.; Dunweg, B.; Borisov, O. V.; Darinskii, A. A. *Macromolecules* **1999**, *32*, 3264−3278.
(13) Chodanowski, P.; Stoll, S. *J. Chem. Phys.* **1999**, *111*, 6069−6081.
(14) Micka, U.; Holm, C.; Kremer, K. *Langmuir* **1999**, *15*, 4033−4044.
(15) Micka, U.; Kremer, K. *Europhys. Lett.* **2000**, *49*, 189−195.
(16) Limbach, H. J.; Holm, C.; Kremer, K. *Europhys. Lett.* **2002**, *60*, 566−572.
(17) Holm, C.; Limbach, H. J.; Kremer, K. *J. Phys.: Condens. Matter* **2003**, *15*, S205−S211.
(18) Limbach, H. J.; Holm, C.; Kremer, K. *Macromol. Symp.* **2004**, *211*, 43−53.
(19) Limbach, H. J.; Holm, C. *J. Phys. Chem. B* **2003**, *107*, 8041−8055.
(20) Heitz, C.; Rawiso, M.; Francois, J. *Polymer* **1999**, *40*, 1637−1650.
(21) Carbajal-Tinoco, M. D.; Williams, C. E. *Europhys. Lett.* **2000**, *52*, 284−290.
(22) Carbajal-Tinoco, M. D.; Ober, R.; Dolbnya, I.; Bras, W.; Williams, C. E. *J. Phys. Chem. B* **2002**, *106*, 12165−12169.
(23) Baigl, D.; Ober, R.; Qu, D.; Fery, A.; Williams, C. E. *Europhys. Lett.* **2003**, *62*, 588−594.
(24) Minko, S.; Kiriy, A.; Gorodyska, G.; Stamm, M. *J. Am. Chem. Soc.* **2002**, *124*, 3218−3219.
(25) Minko, S.; Kiriy, A.; Gorodyska, G.; Stamm, M. *J. Am. Chem. Soc.* **2002**, *124*, 10192−10197.
(26) Kirwan, L. J.; Papastavrou, G.; Borkovec, M. *Nano Lett.* **2004**, *4*, 149−152.
(27) de Gennes, P. G.; Pincus, P.; Velasco, R.; Brochard, F. *J. Phys. (Paris)* **1976**, *37*, 1461.
(28) Chang, R.; Yethiraj, A. *J. Chem. Phys.* **2001**, *114*, 7688−7699.
(29) Chang, R.; Yethiraj, A. *J. Chem. Phys.* **2003**, *118*, 6634−6647.
(30) Tuckerman, M.; Berne, B. J.; Martyna, G. J. *J. Chem. Phys.* **1992**, *97*, 1990−2001.
(31) Martyna, G. J.; Klein, M. L.; Tuckerman, M. *J. Chem. Phys.* **1992**, *97*, 2635−2643.
(32) Martyna, G. J.; Tuckerman, M. E.; Tobias, D. J.; Klein, M. L. *Mol. Phys.* **1996**, *87*, 1117−1157.
(33) Nosé, S. *J. Chem. Phys.* **1984**, *81*, 511−519.
(34) Hoover, W. G. *Phys. Rev. A* **1985**, *31*, 1695−1697.
(35) Dobrynin, A. V.; Rubinstein, M. *Macromolecules* **1999**, *32*, 915−922.
(36) Dobrynin, A. V.; Rubinstein, M. *Macromolecules* **2001**, *34*, 1964−1972.
(37) Stevens, M. J.; Kremer, K. *J. Chem. Phys.* **1995**, *103*, 1669−1690.
(38) Joanny, J. F.; Pincus, P. *Polymer* **1980**, *21*, 274−278.
(39) Luna-Barcenas, G.; Meredith, J. C.; Sanchez, I. C.; Johnston, K. P.; Gromov, D. G.; de Pablo, J. J. *J. Chem. Phys.* **1997**, *107*, 10782−10792.
(40) Grosberg, A. Y.; Khokhlov, A. R. *Statistical Physics of Macromolecules*; AIP Press: New York, 1994.
(41) Winkler, R. G.; Gold, M.; Reineker, P. *Phys. Rev. Lett.* **1998**, *80*, 3731−3734.
(42) Liu, S.; Muthukumar, M. *J. Chem. Phys.* **2002**, *116*, 9975−9982.
(43) Chang, R.; Yethiraj, A. *J. Chem. Phys.* **2002**, *116*, 5284−5298.
(44) Shew, C.-Y.; Yethiraj, A. *J. Chem. Phys.* **1999**, *110*, 676−681.
(45) Mel'nikov, S. M.; Sergeyev, V. G.; Yoshikawa, K. *J. Am. Chem. Soc.* **1995**, *117*, 2401−2408.
(46) Mel'nikov, S. M.; Sergeyev, V. G.; Yoshikawa, K. *J. Am. Chem. Soc.* **1995**, *117*, 9951−9956.
(47) Stoddard, S. D. *J. Comput. Phys.* **1978**, *27*, 291−293.
(48) Allen, M. P.; Tildesley, D. J. *Computer Simulation of Liquids*; Oxford University Press: New York, 1987.
(49) Manning, G. S. *J. Chem. Phys.* **1969**, *51*, 924.
(50) Yethiraj, A. *Macromolecules* **2003**, *36*, 5854−5862.

MA051095Y